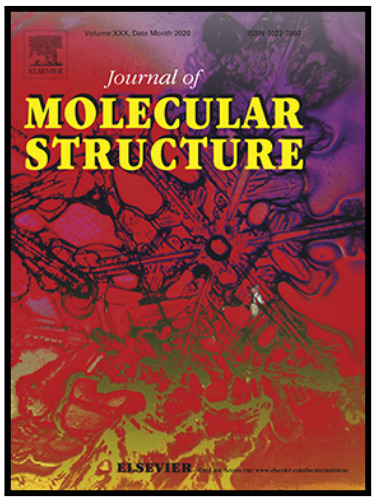

Heteroligand bivalent transition metal complexes with an azo-oxime ligand and 1,10-phenanthroline: synthesis, spectroscopy, thermal analysis, DFT calculations and SOD-mimetic activities

Kerim Serbest , Turan Dural , Mustafa Emirik , Ali Zengin , Özlem Faiz

PII: S0022-2860(20)31893-7
DOI: https://doi.org/10.1016/j.molstruc.2020.129579
Reference: MOLSTR 129579

To appear in: *Journal of Molecular Structure*

Received date: 21 July 2020
Revised date: 22 October 2020
Accepted date: 2 November 2020

Please cite this article as: Kerim Serbest , Turan Dural , Mustafa Emirik , Ali Zengin , Özlem Faiz , Heteroligand bivalent transition metal complexes with an azo-oxime ligand and 1,10-phenanthroline: synthesis, spectroscopy, thermal analysis, DFT calculations and SOD-mimetic activities, *Journal of Molecular Structure* (2020), doi: https://doi.org/10.1016/j.molstruc.2020.129579

Highlights

- Mixed ligand complexes were prepared.
- DFT calculations were performed to assign the experimental spectral data.
- Cu(II) complex shows the most SOD-mimicking activity.

Heteroligand bivalent transition metal complexes with an azo-oxime ligand and 1,10-phenanthroline: synthesis, spectroscopy, thermal analysis, DFT calculations and SOD-mimetic activities

Kerim Serbest[a,*], Turan Dural[a], Mustafa Emirik[a], Ali Zengin[b] and Özlem Faiz[a],

[a] Department of Chemistry, Recep Tayyip Erdogan University, 53100 Rize, Turkey

[b] Pazar Vocational School, Recep Tayyip Erdogan University, 53300 Pazar/Rize, Turkey

Abstract

Novel mononuclear heteroligand transition metal complexes: $[M(HL)(phen)_2]ClO_4$, (M: Mn(II) for **1**, Ni(II) for **2**), $[M(HL)(phen)(ClO_4)]$, (Ni(II) for **3**, Cu(II) for **4**, Zn(II) for **5**) with 2-[(*E*)-(hydroxyimino)methyl]-4-[(*E*)-phenyldiazenyl]phenol, H_2L as primary ligand and 1,10- phenanthroline as bidentate co-ligand(s) in different mole ratios have been synthesized and characterized by using elemental analysis, FTIR, UV-Vis, NMR, MALDI-TOF mass spectrometry and thermal analysis. The complexes (**1, 2**) have distorted octahedral geometry while the complexes (**3**-**5**) have distorted square-pyramidal coordination geometry. In the complexes, the metal ion is coordinated to the deprotonated azo-oxime ligand through the phenolic oxygen atom and nitrogen of the imine. 1,10-Phenanthroline is coordinated to the metal ion through its two N-donors. The thermograms of all the complexes were confirmed the proposed structures. Time-dependent (TD) DFT-based calculations have been also performed for geometric optimization and to assign the experimental vibrational and electronic transition of the complexes. The superoxide-scavenging activities of the complexes were also investigated and IC_{50} values were evaluated. Among the complexes studied, the Cu(II) complex (**4**) exhibits the most activity with the lowest IC_{50} value (2.02 ± 0.15).

Keywords: Vibrational analyses; Electronic transition, TDDFT; Azo dye; SOD.

*Corresponding author. Department of Chemistry, Recep Tayyip Erdogan University, 53100, Rize, Turkey Tel.: +90 464 2236126.

E-mail address: kerimserbest@yahoo.com (K.Serbest).

1. Introduction

The azo-imine ligands contain both azo and imine group and their complexes have been studied for their variety of applications in laser, liquid crystalline displays, textile, leather and plastic industries, corrosion prevention, catalysis, analytical fields, optical storage technologies as well as to treat nuclear wastes [1–3]. The azo ligands have —N=N— linkage between two phenyl rings. Two isomeric forms, energetically stable trans-form and less stable cis-form, are presented in these ligands due to the double bond between the nitrogen atoms [4]. A great number of azo compounds are used in pharmaceuticals and cosmetics although some azo compounds were reported as toxic [5]. The azo-imine complexes also find important applications in medicine due to their useful biological activities including anti-microbial, antitumor, anticancer, anti-fungicidal [1,6].

The transition metal complexes based on 1,10-phenanthroline (phen) and its derivatives are widely studied due to antitumor, catalytic, redox, photochemical, and photophysical properties [7–10]. Superoxide radical anions ($O_2^{\cdot -}$) cause oxidative damage of the cells resulting DNA damage, aging, and many other disease formations as cancer [11]. Phenanthroline containing complexes has been reported to be effective for the scavenging of the superoxide radicals [12,13]. Superoxide dismutases (SODs) are metalloenzymes

containing transition metals such as Fe, Mn, Cu/Zn, and scavenge catalytically the superoxide radicals generated by so many spontaneous and enzymatic oxidations in aerobic organisms [14,15]. SODs are inefficient in case of oxygen burst in vivo while they are very efficient in the dismutation of superoxide radicals into hydrogen peroxide and oxygen, under normal conditions [16]. SOD as a metalloprotein has too high molecular weight to pass the cell membranes [17]. Therefore, we are interested in developing synthetic SOD mimics. The critical factors for the effectiveness of mimics are stability, membrane permeability, and low molecular weight. Phenanthroline has two nitrogen donors to coordinate and form stable structures. The azo-imine ligands have a great ability to coordinate with the transition metals and form high stable structures [1]. So, the mixed ligand complexes with their low molecular weight and stabilities of azo-imine and phenanthroline ligands have been seen as good candidates for SOD mimics.

In the present work, we report the synthesis, characterization, quantum chemical assignment of experimental IR and UV–Vis spectra and SOD mimetic activities of a series of Mn(II), Ni(II), Cu(II), and Zn(II) complexes (**1-5**) derived from azo-imine ligand 2-[(*E*)-(hydroxyimino)methyl]-4-[(*E*)-phenyldiazenyl]phenol, H_2L and 1,10-phenanthroline (phen) as co-ligand (Figure 1).

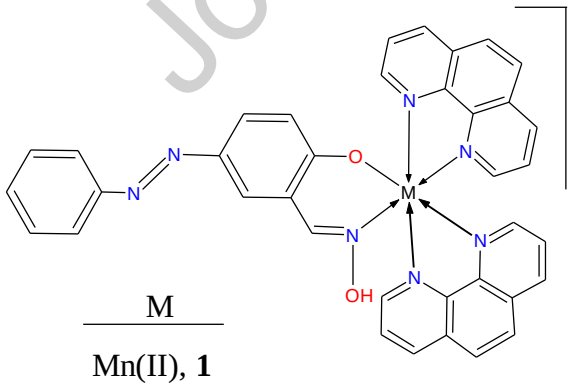

M

Mn(II), **1**

Ni(II), **2**

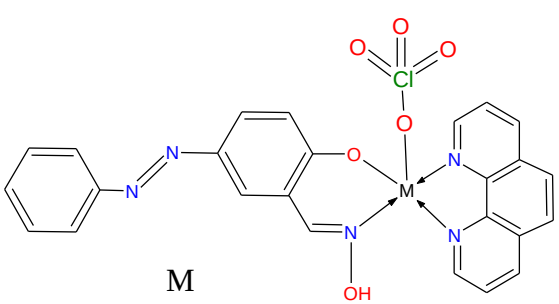

M

Ni(II), **3**

Cu(II), **4**

Zn(II), **5**

Figure 1. The proposed structures of the complexes (**1-5**).

2. Experimental

2.1. Materials and Methods

1,10-Phenanthroline monohydrate (Merck), metal perchlorates (Merck), and all the solvents were of reagent grade and used without any further purification. 2-[(*E*)-(hydroxyimino)methyl]-4-[(*E*)-phenyldiazenyl]phenol, H_2L was synthesized in two steps by previously reported procedure [18].

2.2. Measurements

Fourier transform infrared (FT-IR) spectra were recorded on a Perkin Elmer Spectrum 100 spectrometer equipped with an ATR apparatus. Elemental analyses were performed using a LECO truspect analyzer at the Central Research Laboratory of Recep Tayyip Erdogan (RTE) University. MALDI-TOF mass spectroscopy in a DHB matrix was investigated on a Bruker Microflex LT at the Gebze Institute of Technology for the complex. The ^{1}H NMR spectra were recorded on an Agilent Technologies 400/54 spectrometer at the Central Research Laboratory of RTE University. UV–Vis spectra were recorded on a SpectroScan 60DV UV-*vis*. spectrophotometer. Magnetic susceptibility and thermogravimetric data were collected by using Sherwood MK-1 and SII 6300 TG/DTA, respectively.

2.3. Determination of SOD-like activity

The SOD-like activities of the heteroligand transition metal complexes at different concentrations were evaluated by the indirect NBT-DMSO method in which alkaline DMSO was used as a source of superoxide radical ($O_2^{\cdot -}$) and nitroblue tetrazolium chloride (NBT) was used as $O_2^{\cdot -}$ scavenger [19–21]. 0.2 mL sample was mixed with a solution containing 1.0

mL of 0.2 M potassium phosphate buffer (pH 8.6) and 0.5 mL of 5 mM of alkaline DMSO solution (prepared just before use) to give a final volume of 1.7 mL. The absorbance was measured at 540 nm against a sample containing all the reagents above except DMSO was used instead of alkaline DMSO.

2.4. Computational Details

All calculations were performed using the Gaussian 09 [22] program. Density functional theory (DFT) were used for all the theoretical calculations. Geometry optimizations were carried out at the B3LYP functional combined with basis sets 6–311 ++ G(d,p) for nonmetal atoms and LANL2DZ for metal atoms and an effective core potential (ECP) was used for metal atoms [23]. The gas-phase vibrational frequencies were calculated at the same level of theory. Frequency analysis calculations have characterized the structures to be the minima (no imaginary frequency). The fundamental vibrational modes were analyzed employing the Potential Energy Distribution (PED) using the VEDA4X program [24]. The Time Dependent-Density Functional Theory (TD-DFT) calculations of both ligands and metal complexes were performed using Gaussian 09. The electronic excitations were calculated at the same level of theory by using TD-DFT combined with a conductor-like polarizable continuum model (CPCM) in the implicit solvent of DMSO ($\varepsilon = 46.826$) [25]. GAUSSSUM 3.0 [26] was used to attribute the excitation energies of experimental UV-Vis bands and analyze the fractional contributions to each molecular orbital. The optimized geometries have been considered for the TD-DFT calculation. All generated molecular orbitals and optimized geometry were visualized by Gauss view 5.0.

*2.5. Synthesis of the complexes (**1-5**)*

A general method for the synthesis of complexes has been followed. An ethanolic solution of metal(II) perchlorates ($Mn(ClO_4)_2 \cdot 6H_2O$, $Ni(ClO_4)_2 \cdot 6H_2O$, $Cu(ClO_4)_2 \cdot 6H_2O$ and $Zn(ClO_4)_2 \cdot 6H_2O$) (1 mmol) to a solution of 2-[(*E*)-(hydroxyimino)methyl]-4-[(*E*)-phenyldiazenyl]phenol, H_2L (1 mmol) in 15 mL anhydrous ethanol, neutralized with an ethanolic solution of NaOH and the mixture was stirred for an hour at room temperature. Then, the solution of 1,10-phenanthroline monohydrate (2.0 mmol for **1** and **2**; 1.0 mmol for **3-5**) in 10 mL anhydrous ethanol was dropped to the reaction mixture, the color change was observed immediately. The mixture was stirred for two days at room temperature and the resulting precipitate was collected by filtration. It was recrystallized from hot DMF-EtOH (ca. 1:5) mixture, washed with water and ethanol, respectively, and dried in an oven 50 °C and then over $CaCl_2$ in vacuo. It wasn't obtained any suitable crystals for X-ray diffraction studies though our great efforts.

*2.5.1. Synthesis of [Mn(HL)(phen)$_2$](ClO$_4$), (**1**)*

Analytical and physical data; Yield 0.465 g (62%). mp 299-301 °C (dec.). Color: Greenish brown. Anal. Calc. for $C_{37}H_{26}ClN_7O_6Mn$: C, 58.86; H, 3.47; N, 12.99. Found C, 59.04; H, 3.55; N, 13.16. UV-Vis. λ_{max}, nm (ε, M^{-1} cm^{-1}) in DMF: 337 (21960); 397 (25800). FT-IR (cm^{-1}): 1626, 1592 ν(C=N); 1519, 1496 ν(-C═C-); 1423 ν(N═N); 1304 ν(C-O); 1073 $\nu(ClO_4)^-$; 724, 842 (phen). Molar conductivity ($\Omega^{-1}cm^2mol^{-1}$) 63. μ_{eff} B.M. (298 K): 5.88 (for per metal ion). MALDI-TOF MS (m/z): Calcd for $C_{37}H_{26}ClMnN_7O_6$: 754.1; Found: 754.3 $[M]^+$, Calcd for $C_{25}H_{18}MnN_5O$: 459.4; Found: 459.7 $[M-(phen+ClO_4+OH)]^+$.

*2.5.2. Synthesis of [Ni(HL)(phen)$_2$](ClO$_4$), (**2**)*

Analytical and physical data; Yield 0.485 g (64%). mp 269-273 °C (dec.). Color: Green. Anal. Calc. for $C_{37}H_{26}ClN_7O_6Ni$: C, 58.57; H, 3.45; N, 12.92. Found C, 58.28; H, 3.49; N, 13.09. UV-Vis. λ_{max}, nm (ε, M^{-1} cm^{-1}) in DMF: 268 (23050); 351 (24490); 435 (4810). FT-IR (cm^{-1}): 3600-3200 ν(OH); 1626, 1604 ν(C=N); 1518, 1475,1422 ν(-C═C-); 1410 ν(N═N); 1301 ν(C-O); 1076 ν$(ClO_4)^-$; 721, 842 (phen). Molar conductivity ($\Omega^{-1}cm^2mol^{-1}$) 76. μ_{eff} B.M. (298 K): 3.19 (for per metal ion). MALDI-TOF MS (m/z): Calcd for $C_{37}H_{26}N_7NiO_2$: 658.1; Found: 657.7 $[M\text{-}ClO_4]^+$, Calcd for $C_{31}H_{24}N_6NiO_2$: 570.2; Found: 570.7 $[M\text{-}(C_6H_5N+ClO_4)]^+$.

*2.5.3. Synthesis of [Ni(HL)(phen)(ClO$_4$)], (**3**)*

Analytical and physical data; Yield 0.274 g (48%). mp 267-274 °C (dec.). Color: Goldenroad. Anal. Calc. for $C_{25}H_{18}ClN_5O_6Ni$: C, 51.90; H, 3.14; N, 12.10. Found C, 51.68; H, 3.32; N, 11.96. UV-Vis. λ_{max}, nm (ε, M^{-1} cm^{-1}) in DMF: 295 (31790); 365 (20460); 448 (1360). FT-IR (cm^{-1}): 3640-3200 ν(OH); 1644, 1604 ν(C=N); 1548, 1475 ν(-C═C-); 1405 ν(N═N); 1301 ν(C-O); 1145, 1110 ν$(ClO_4)^-$; 763, 825 (phen). Molar conductivity ($\Omega^{-1}cm^2mol^{-1}$) 25. μ_{eff} B.M. (298 K): 2.81 (for per metal ion). MALDI-TOF MS (m/z): Calcd for $C_{25}H_{19}ClN_5NiO_6$: 578.0; Found: 577.8 $[M+H]^+$.

*2.5.4. Synthesis of [Cu(HL)(phen)(ClO$_4$)], (**4**)*

Analytical and physical data; Yield 0.563 g (96%). mp 253-259 °C (dec.). Color: Khaki. Anal. Calc. for $C_{25}H_{18}ClN_5O_6Cu$: C, 51.47; H, 3.11; N, 12.00. Found C, 51.74; H, 3.32 N, 11.81. UV-Vis. λ_{max}, nm (ε, M^{-1} cm^{-1}) in DMF: 331 (29220); 366 (32290); 437 (26700). FT-IR (cm^{-1}): 3650-3180 ν(OH); 1648, 1613 ν(C=N); 1522, 1483, 1432 ν(-C═C-); 1405 ν(N═N); 1315 ν(C-O); 1150, 1111, 1067 ν$(ClO_4)^-$; 765, 827 (phen). Molar conductivity ($\Omega^{-1}cm^2mol^{-1}$)

16. μ_{eff} B.M. (298 K): 2.04 (for per metal ion). MALDI-TOF MS (m/z): Calcd for $C_{25}H_{18}CuN_5O_2$: 483.0; Found: 482.7 $[M\text{-}ClO_4]^+$, Calcd for $C_{32}H_{24}CuN_5O_6$: 637.1; Found: 637.8 $[M+DHB\text{-}ClO_4]^+$.

*2.5.5. Synthesis of [Zn(HL)(phen)(ClO_4)], (**5**)*

Analytical and physical data; Yield 0.285 g (49%). mp 295 °C (dec.). Color: Brownish yellow. Anal. Calc. for $C_{25}H_{18}ClN_5O_6Zn$: C(51.30%) H(3.10%) Cl(6.06%) N(11.97%) C, 51.30; H, 3.10; N, 11.97. Found C, 51.27; H, 3.16; N, 12.13. UV-Vis. λ_{max}, nm (ε, M^{-1} cm^{-1}) in DMF: 350 (12310); 435 (13530). FT-IR (cm^{-1}): 3650-3180 ν(OH); 1624 1587 ν(C=N); 1518, 1475, 1432 ν(-C═C-); 1396 ν(N═N); 1293 ν(C-O); 1143, 1102, 1070 ν$(ClO_4)^-$; 721, 817 (phen). ^{1}H NMR ($CDCl_3$, δ ppm): 10.98 s. (1H, OH), 9.02 s. (1H, HC=N), 8.49 s. (2H, Ar), 7.96-7.79 m. (5H, Ar), 7.46-7.21 m. (8H, Ar), 6.62 d. (1H, Ar, J=8,0 Hz), 1.58 s. (H_2O in solvent); Molar conductivity ($\Omega^{-1}cm^2mol^{-1}$) 44. μ_{eff} B.M. (298 K): dia. MALDI-TOF MS (m/z): Calcd for $C_{25}H_{18}ClN_5O_6Zn$: 583.0; Found: 583.3 $[M]^+$.

MALDI-TOF MS, m/z (%): 583.3 (100 a.u.) $[M\text{-}2H]^+$. C25H18ClN5O6Zn

3. Results and discussion

3.1. NMR spectra

The proton NMR spectra of Zn(II) complex, **5** has been recorded in $CDCl_3$ solution using tetramethylsilane (TMS) as an internal standard (Figure 2). The chemical shifts of the different types of protons of Zn(II) complex is given in the experimental section and the

spectrum was compared with that of primary 2-[(*E*)-(hydroxyimino)methyl]-4-[(*E*)-phenyldiazenyl]phenol, H_2L. While the signal of C=N-OH at 11.60 ppm shifted to 10.98 ppm, the phenolic OH signal at 10.96 ppm is completely disappeared. The singlet of oxime proton at 10.98 ppm was disappeared after D_2O was added. The singlet of HC=N at 8.39 ppm shifted to 9.02 ppm. Lowfield shift of the imine proton signal, a decrease in the acidity of oxime proton, and the disappearance of the phenolic proton signal indicate the coordination of H_2L to Zn(II) ion through the nitrogen of imine and the phenolic oxygen atoms, respectively. Comparing with the proton NMR spectra of the primary ligand, an increase in the integrated intensities at the region of 6.5-8.5 ppm was observed. The integrated intensities of the aromatic protons show the presence of a phenanthroline co-ligand.

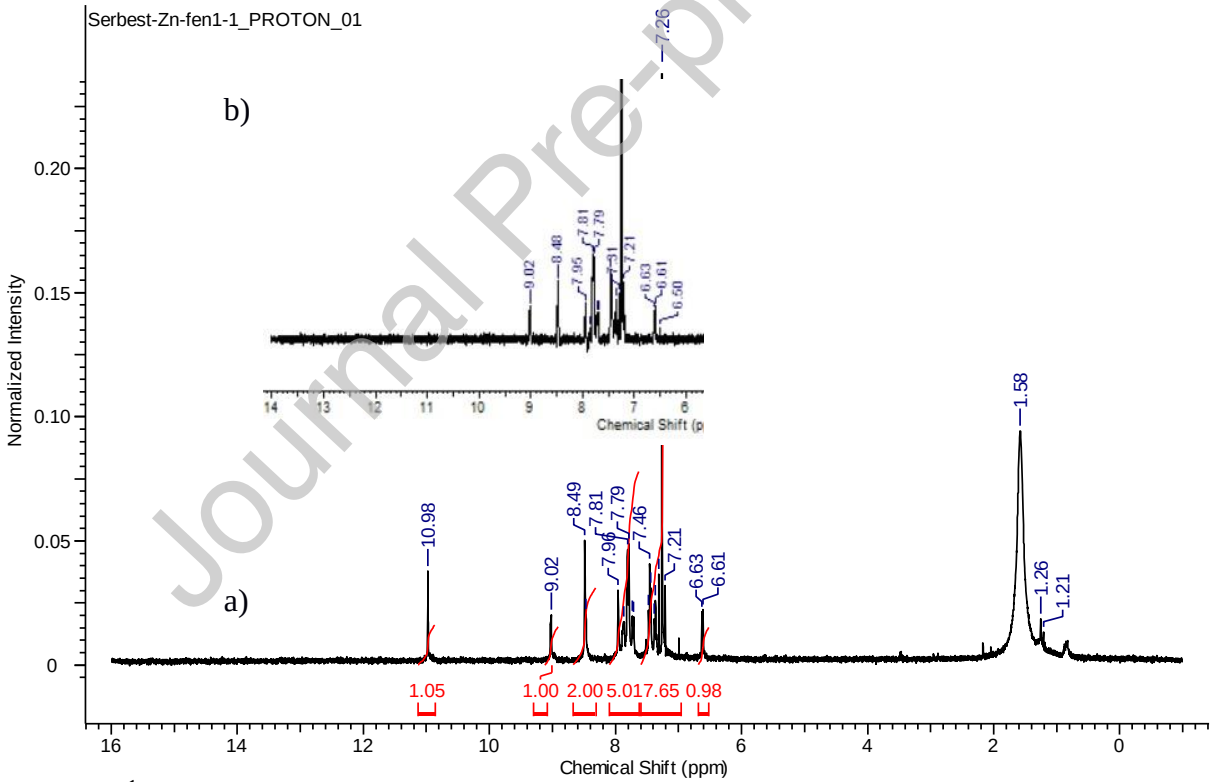

Figure 2. ^{1}H NMR spectra of Zn(II) complex, **5** in $CDCl_3$ (a) before the addition of D_2O, and (b) after the addition of D_2O.

3.2. Theoretical calculations

3.2.1. Molecular Structures

The theoretical calculations have been performed for the free ligand and the complexes (**1-5**) in order to obtain satisfactory information regarding the structural characteristics and the fundamental spectroscopic properties. The optimized molecular structures with bond lengths, overlap populations, and bond orders between metal and donor atoms were given in Figures 3-8.

In these structures, the coordination geometry around metal atoms is described as octahedral geometry by four nitrogens of two phenanthroline ligands and one oxygen and one nitrogen of imine of the primary oxime ligand in compound **1** and **2**. The coordination geometry around a metal atom of complex **3**, **4**, and **5** are described as distorted square pyramidal by two nitrogens of phenanthroline group, one oxygen of perchlorate, one nitrogen, and one oxygen of oxime ligand.

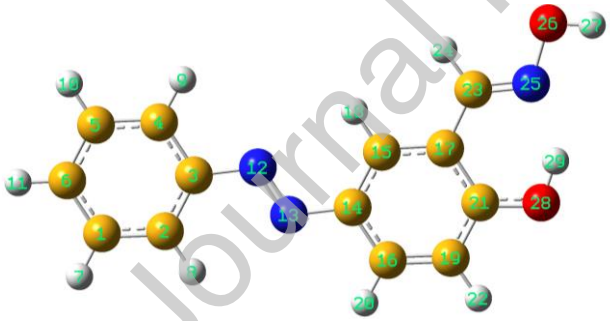

Figure 3. Optimized molecular structure of the free ligand.

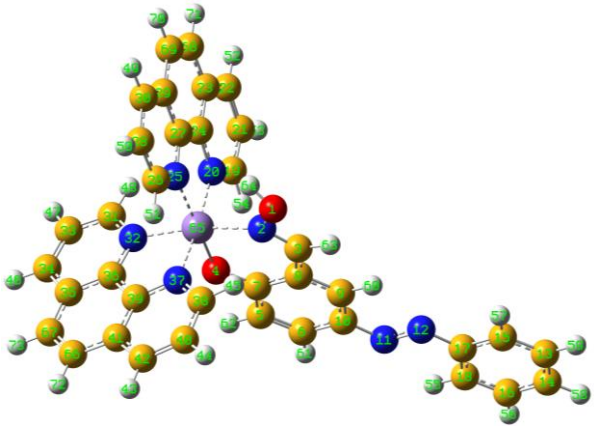

Bond	Length(A)	Overlap Population	Bond order
Mn65-N2	1.99	0.11	0.35
Mn65-O4	1.94	0.23	0.60
Mn65-N25	2.06	0.08	0.30
Mn65-N20	2.04	0.09	0.32
Mn65-N32	2.05	0.08	0.31
Mn65-N37	2.05	0.08	0.32

Figure 4. Optimized molecular structure of complex **1**.

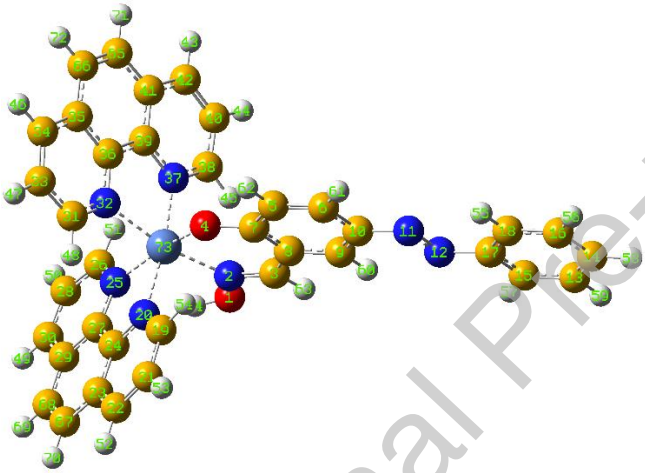

Bond	Length (A)	Overlap Population	Bond order
Ni73-N2	2.05	0.10	0.31
Ni73-O4	1.99	0.21	0.54
Ni73-N25	2.13	0.08	0.25
Ni73-N20	2.10	0.07	0.26
Ni73-N32	2.10	0.07	0.26
Ni73-N37	2.10	0.06	0.26

Figure 5. Optimized molecular structure of complex **2**.

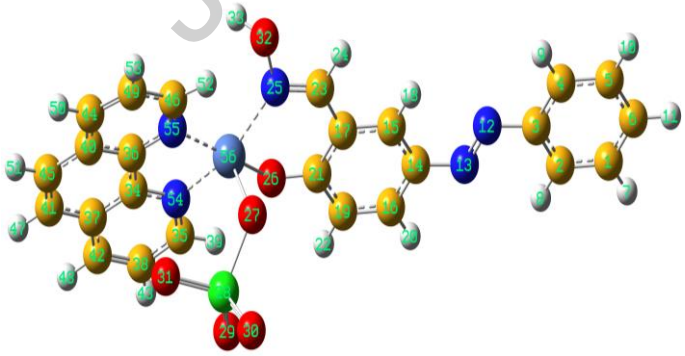

Bond	Length(A)	Overlap Population	Bond order
Ni56-N25	2.04	0.19	0.447
Ni56-O26	1.98	0.18	0.517
Ni56-O27	1.99	0.16	0.538
Ni56-N54	2.06	0.15	0.416
Ni56-N55	2.13	0.14	0.392

Figure 6. Optimized molecular structure of complex **3**.

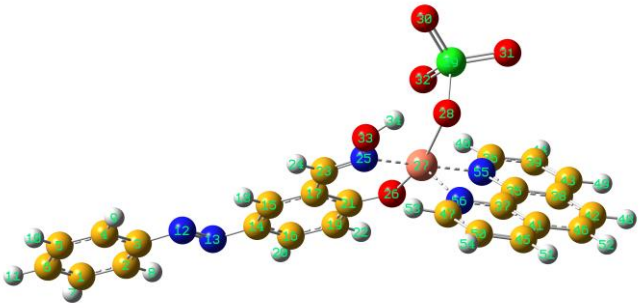

Bond	Length(A)	Overlap Population	Bond order
Cu27-N25	1.96	0.18	0.45
Cu27-O26	1.95	0.22	0.60
Cu27-O28	2.16	0.13	0.35
Cu27-N55	2.01	0.15	0.43
Cu27-N56	2.25	0.11	0.30
Cu27-O32	2.81	0.07	0.13

Figure 7. Optimized molecular structure of **4**.

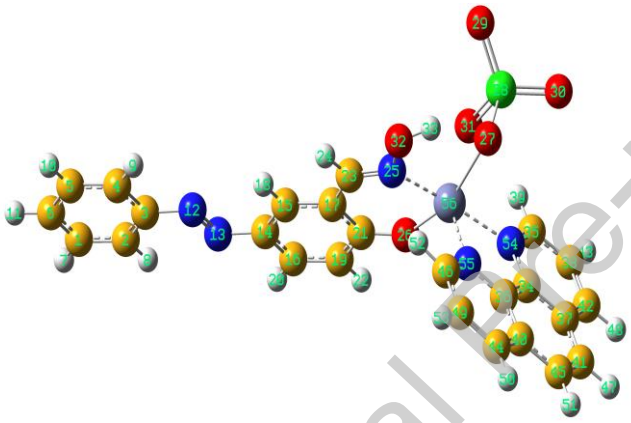

Bond	Length(A)	Overlap Population	Bond order
Zn56-N25	2.13	0.15	0.32
Zn56-O26	1.99	0.19	0.42
Zn56-O31	2.24	0.13	0.27
Zn56-O27	2.38	0.10	0.21
Zn56-N54	2.17	0.12	0.28
Zn56-N55	2.22	0.11	0.26

Figure 8. Optimized molecular structure of **5**.

3.2.2. Vibrational assignments

IR spectra (4000-650 cm^{-1}) of the compounds were generally obtained using the FT-ATR technique. The obtained spectra were evaluated considering the azo derivative oxime ligand used as the starting compound and the IR spectrum of the 1,10-phenanthroline ligand. The theoretical IR spectra of the ligand and all complexes were calculated using the DFT / B3LYP method to assign the experimental signals. The selected vibrations and corresponding functional groups were given in Table 1.

The vibrations observed at 3403, 1393, and 1265 cm^{-1} in the IR spectrum of the azo-oxime ligand were assigned to the oscillation vibrations of the oxime protons (C=N—OH), —N=N— and C—O, respectively. Due to the possible intermolecular and intramolecular hydrogen bonds that can be observed in the ligand structure, the tensile vibrations of the expected phenolic OH protons at a lower frequency than the tensile vibrations of the oxime OH protons could not be observed.

The broad bands observed at approximately 3600-3200 cm^{-1} in the IR spectra of all the complexes were attributed to the oxime O—H vibrations. Besides the phenolic OH stretch was disappeared in all complexes, in the IR spectrum of the azo-oxime ligand, the intense of C—O vibrations observed at 1265 cm^{-1} was shifted to the upper wave number in the complexes (1315-1293 cm^{-1}) and the intensity was decreased compared to the free ligand. It can be seen as evidence of C—O moiety of ligand binds to metal centers. The vibration band belonging to the vibration of the imine C=N observed at a medium intensity at 1621 cm^{-1} in the spectrum of the azo-oxime ligand shifted to the upper wave number (1624-1648 cm^{-1}) and the intensity of this band decreased in the complexes [16,27,28]. It is obvious that in the spectrum of the phenanthroline derivatives complexes, the imine (C=N) vibrations of the phenanthroline ligand shifted to lower frequencies (1613-1587 cm^{-1}). Shifts in the up and down frequencies of the hydroxyl imine (C=NOH) and the imine of phenanthroline vibrations were attributed to the coordination of the metal ion to the azo-oxime and phenanthroline ligands over the imine nitrogens. In addition to the C=C vibrations observed in the region of about 1520 and 1420 cm^{-1} in the phenanthroline complexes, the bands belonging to the characteristic out-of-plane C—H bending observed in 721-765 and 817-842 cm^{-1} were attributed to the phenanthroline unit [29,30]. The obtained spectral data indicate that while the azo-oxime ligand is mostly coordinated to the metal via the imine and phenolic oxygen, 1,10-phenanthroline is coordinated through the nitrogen atoms.

The perchlorate ion has a general tetrahedron geometry and its point group is T_d, having four normal modes of vibration (v_1-v_4). The asymmetrical stretching (v_3, 1110 cm^{-1}) and asymmetrical bending (v_4, 626 cm^{-1}) modes are only IR active [31,32]. In general, asymmetrical stretching (v_3) and asymmetrical bending (v_4) are observed in the infrared spectra of ionic perchlorates. The former appearing as a very broad strong band is very diagnostic and confirms the uncoordination of the perchlorate ion in complex **1**, and **2** (See the supplementary file, Fig. S12 and S13) [33]. Because the perchlorate group is involved in partial covalent bonding between one of its oxygen atoms and central metal ion, the asymmetrical stretching band (v_3, 1110 cm^{-1}) splits into two bands due to the fact that the symmetry of the perchlorate ion is lowered to C_{3v}. The bands are 1110, 1068 cm^{-1} for **3**, 1111, 1067 cm^{-1} for **4**, 1102, 1070 cm^{-1} for **5** (Fig. S14-S16). The splitting confirms the monodentate coordination of the perchlorate ion (Table 1) [32].

Table 1. Selected vibrational frequencies (observed and calculated) of synthesized compounds.

Comp.		ν(C=N-OH)	ν(C-H)	ν(C=N)	Phen	ν(C=C)	ν(N=N)	ν(C–O)	ν(ClO_4)
Ligand	Exp.	3403	3150-3000	1621	_	1569	1393	1265	_
	Theo.	3291(Ph), 3666	3074-2982	1654*	_	1621-1590	1514	1289	_
1	Exp..	_	3100-3050	1626, 1592*	724,842	1519,1496	1423	1304	1073
	Theo.	3501	3106-3023	1614, 1605*	735, 872	1512-1634	1422	1299	_
2	Exp.	3670-3200[a]	3100-3000	1626, 1604*	721,842	1518,1475,1422	1410	1301	1076[a]
	Theo.	2885	3093-3005	1620, 1590*	741, 873	1634-1431	1436	1245	_
3	Exp.	3640-3200[a]	3150-3000	1644, 1604*	763,825	1548,1475	1405	1301	1110,1068
	Theo.	3493	3129-3038	1655, 1600*	738,805	1544-1643	1417	1323	_
4	Exp.	3650-3180[a]	3200-3050	1648, 1613*	765,827	1522,1483,1432	1405	1315	1111,1067
	Theo.	3164	3132-3043	1632,1646*	756, 803	1357-1639	1421	1302	_
5	Exp.	3650-3180[a]	3100-3050	1624, 1587*	721,817	1518,1475,1422	1396	1293	1102,1070
	Theo.	3240	3092-2998	1623, 1634*	740, 872	1428-1629	1405	1337	_

(a: broad, Exp.: experimentally observed, Theo.: Theoretically calculated, *: Phen ν(C=N))

3.2.3. UV-Vis spectra

Experimental absorption bands were interpreted using theoretical data calculated by TDDFT/CPCM method in the implicit solvent medium of DMSO. Some theoretically obtained wavelengths and corresponding excitations and their characters were given in Supplementary (Table S1-S5) with experimentally observed wavelengths.

In the electronic spectrum of the Mn (II) complex (**1**), experimentally observed bands at 337 and 397 nm were attributed to the π→π* and d →n, π* metal to ligand charge transitions (MLCT). The band at 337 nm was generally assigned to H-8(A,B)→L(A)/ L+1(A,B), H(A)→L(A), H(A)→L+4(A), H-1(B)→L+6(B) transition and interpreted as π→π* character according to molecular orbital contributions. The second band at 397 nm was theoretically assigned to H(B)→L+2(B)/L+3(B)/L+4(B)/L+5(B), H-1(B)→L+1(B)/L+2(B)/L+3(B), H-1(A)→L+5(A), H-2(A)→L+1(A)/L+2(A) transition and characterized as MLCT, since H-1(A), H-2(A), H-1(B), H(B) molecular orbitals are mainly located on the metal atom. The experimental and theoretical electronic transitions with their assignments were given in Table S2. Three separate bands were observed at 268, 351, and 435 nm in the electronic spectrum of the complex **2**. According to theoretical data, the first band is weighted to π→π* and n→π* transitions and minor contribution of LMCT transitions. The second and third bands attributed to π→π * and d→d transitions, respectively. In the electronic spectrum of the complex **3**, the band observed at 295 was attributed to LMCT transitions and the bands at 448 nm and 365 nm were attributed to π→π* and minor contribution of LMCT. Three bands at 331, 366, and 437 nm observed in the electronic spectrum of the Cu(II) complex (**4**) were dominated by π→π*, n→π*, and LMCT transitions. Two bands at 350 and 435 nm observed in the electronic spectrum of the Zn(II) complex (**5**) were dominated by π→π* and n→π* transitions. Experimental absorption bands, theoretical electronic transitions, and their character assignments in detail were tabulated at Table S1-S5 in Supplementary.

3.3. Thermal stabilities

The thermal decomposition processes for the complexes (**1-5**) were studied by TG/DTG/DTA analysis to get information about their thermal stabilities and determine the metal/ligand ratio. The TG curves of the complexes (**1-5**) were shown in Figure 9 (see Supplementary, Fig. S1-S5 for the DTA_{max}) and obtained data were presented in Table 2. The overall residues in thermograms of the complexes are in agreement with the proposed structures and their stoichiometries.

Mn(II) complex, **1** has one step decomposition at 130-580 °C with the weight lost 90.2% (calc. 90.6%). The mass lost is assigned to the removal of HL, two phenanthroline molecules, and ClO_4-O. We assumed that the final residue left at the end of the thermal decomposition process above 578°C is mainly MnO, the amount of the residue is 10.8% (calc. 9.4%) and suitable for the proposed structure.

The TG curve of the Ni(II)-HL-phenanthroline complex, **2** (1:1:2) showed three separated decomposition steps within the range of 25-685°C. The endothermic first step at 25-88°C is assigned to dehydration of the adsorbed water with a mass loss of 2.6% (calc. 2.3%). The complex **2** decomposed rapidly in the second step at 204-394°C with a mass loss of 23.4% (calc. 23.2%). The mass loss is assigned to the removal of a phenanthroline molecule. The removals of the second phenanthroline, HL, and ClO_4-O occurred in the third step at 394-685°C with a mass loss of 68.7% (calc. 69.0%). The final residue left is NiO with a mass of 9.3% (calc. 9.8%).

The TG curve of the Ni(II)-HL-phenanthroline complex, **3** (1:1:1) showed three separated decomposition steps within the range of 25-695°C. The endothermic first step at 25-75°C is assigned to dehydration of 0.8 mol adsorbed water with a mass loss of 2.5% (calc. 2.5%). The complex **3** decomposed rapidly in the second step at 223-451°C with a mass loss of 29.5%

(calc. 29.4%). The mass loss is assigned to the removal of a phenanthroline molecule. The removals of the HL and ClO_4-O occurred in the third step at 451-695°C with a mass loss of 55.4% (calc. 52.9%). The final residue left is NiO with a mass of 12.8% (calc. 12.9%).

Cu(II) complex, **4** has three endothermic decomposition steps at 25-628 °C. The first step at 25-58°C is assigned to dehydration of 0.8 mol adsorbed water with a mass loss of 2.6% (calc. 2.6%). The second step at 204-293°C is assigned to the removals of phenanthroline molecule and C_6H_5 with a mass loss of 43.4% (calc. 43.0%). The identification of step 2 and 3 is difficult because not only phenanthroline but also HL decomposed at the same time in the second step. The third step at 311-628°C is assigned to the removals of $C_7H_7ClN_3O_5$ with mass loss of 40.2% (calc. 41.4%). The final residue left is CuO with a mass of 15.6% (calc. 13.3%).

Zn(II) complex, **5** has one step decomposition at 217-605 °C with the weight lost 85.1.2% (calc. 86.1%). The mass loss is assigned to the removal of the HL+phenanthroline +ClO_4-O molecule. We assumed that the final residue left at the end of the thermal decomposition process above 605°C is mainly ZnO, the amount of the residue is 14.9% (calc. 13.9%).

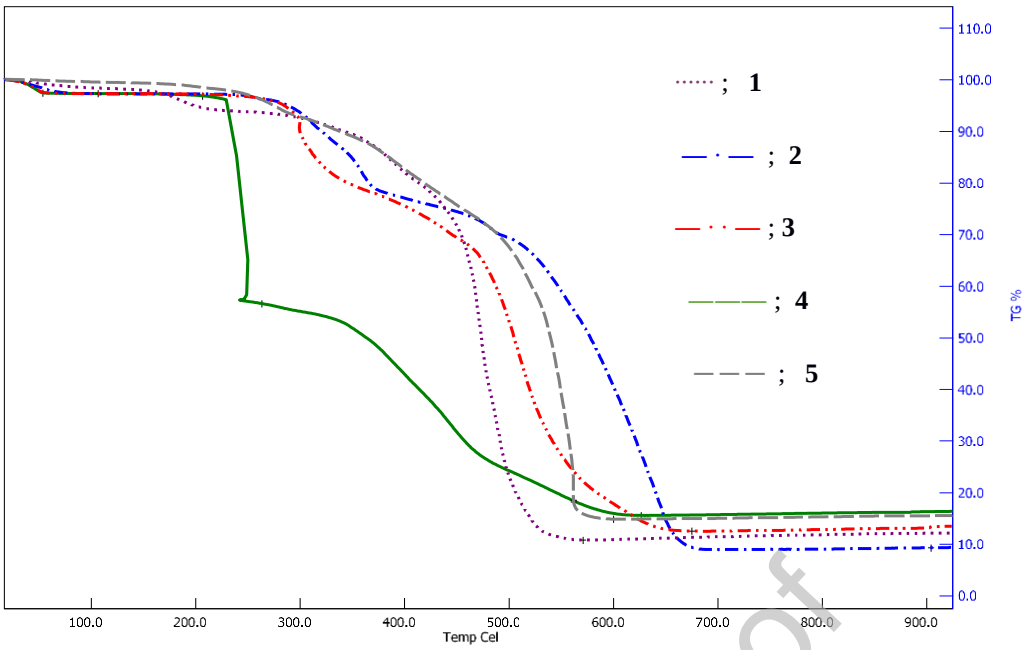

Figure 9. TG curves of the complexes (**1-5**).

Table 2. Thermal analysis data of the complexes.

Comp.	Decom. Step(s)	Decom. Temp., °C	DTA_{max}, µV	Group lost, mass loss %, exp. (calc.)	Residue formula, Residue %,exp. (calc.)
1	1	130-580	189(+), 466(+), 482(+)	HL +2phen+ClO_4-O 90.2 (90.6)	MnO, 10.8 (9.4)
2	1	25-88	54(-)	H_2O, 2.6, (2.3)	$[Ni(HL)(phen)_2]ClO_4$, 97.4 (97.7)
	2	204-394	256(+), 359(+)	Phen, 21.4 (23.2)	$[Ni(HL)(phen)]ClO_4$, 76.0(76.8)
	3	394-685	480(+), 614(+)	HL +phen+ClO_4-O 67.0(68.4)	NiO, 9.3 (9.8)
3	1	25-75	48(-)	0.8H_2O, 2.5, (2.5)	$[Ni(HL)(phen)]ClO_4$, 97.5 (97.5)
	2	223-451	300(+), 436(+)	Phen, 29.5 (29.4)	$[Ni(HL)]ClO_4$, 68.0(68.1)
	3	451-695	502(+), 611(+)	HL +ClO_4-O 55.4 (52.9)	NiO, 12.8 (12.9)
4	1	25-58	48(-)	0.8 H_2O, 2.6, (2.6)	$[Cu(HL)(phen)]ClO_4$, 97.4 (97.4)
	2	204-293	250(+), 272(+)	Phen+C_6H_5 43.4(43.0)	$C_7H_7ClN_3O_6Cu$ 54.0 (54.7)
	3	311-628	381(+),441(+),543(+)	$C_7H_7ClN_3O_5$ 40.2(41.4)	CuO, 15.6 (13.3)
5	1	217-605	323(+), 545(+),	HL +phen+ClO_4-O 85.1(86.1)	ZnO, 14.9 (13.9)

3.4. SOD activity studies

SOD is an antioxidant enzyme that catalyzes the dismutation of the superoxide radical anions ($O_2^{\cdot -}$) generated during the metabolic activities of cells [34]. The catalytic activity of the metal complexes towards superoxide radical anions were measured. IC_{50} is defined as the concentration of the metal complexes produces 50% inhibition of NBT reduction [16]. SOD-like activity provided a means to reveal potential SOD mimics [35]. Many metal complexes have the ability to dismutate the superoxide radical anions [36–38]. The complex concentration which is required to yield 50% inhibition of the reduction of NBT of $[Mn(HL)(phen)_2]ClO_4$, $[Ni(HL)(phen)_2]ClO_4$, $[Ni(HL)(phen)(ClO_4)]$, $[Cu(HL)(phen)(ClO_4)]$, $[Zn(HL)(phen)(ClO_4)]$ are 8.36 ± 0.55, 6.00 ± 0.36, 2.80 ± 0.19, 2.02 ± 0. 15 and 2.90 ± 0.11, respectively (Table 3). The copper(II) complex has the best activity with the lowest value (2.02 µM). All the obtained IC_{50} values of the complexes are higher than the value reported for the native enzyme (IC_{50} = 0.04 µM) [36] but lower than the values exhibited for some reported metal complexes [12,20,38]. The difference in activity of the complexes is determined by the geometry and redox behavior of the metal center. So, the lower activities than the others are expected for the Mn(II) and Ni(II) complexes (**1** and **2**) due to their saturated geometries. Due to the possibility of a strong axial bond between the metal center and superoxide ion, the greater activities are observed in the complexes (**3-5**) having penta-coordination. Among them, it is not surprising that the copper(II) complex is the most active due to the redox potential. The dismutation potential of the synthesized metal complexes was lower than the native enzyme but instability and denaturation under environmental conditions limit the native enzyme's commercial applications. The synthesized metal complexes with high stability and low molecular weight make them be good candidates as SOD mimics.

Table 3. The SOD-like activities of the complexes (**1-5**).

Complex	**[a]IC_{50} (μM)**
$[Mn(HL)(phen)_2]ClO_4$, **1**	8.36 ± 0.55
$[Ni(HL)(phen)_2]ClO_4$, **2**	6.00 ± 0.36
$[Ni(HL)(phen)(ClO_4)]$, **3**	2.80 ± 0.19
$[Cu(HL)(phen)(ClO_4)]$, **4**	2.02 ± 0. 15
$[Zn(HL)(phen)(ClO_4)]$, **5**	2.90 ± 0.11

[a]IC_{50} is defined as the concentration of the metal complexes produces 50% inhibition of NBT reduction

4. Conclusion

Five novel mononuclear heteroligand transition metal complexes with 2-hydroxy-5-[(E)-(4-phenyl) diazenyl] benzaldehyde oxime, H_2L as the primary ligand, and 1,10-phenanthroline as bidentate co-ligand(s) in different mole ratios have been reported. The information obtained from physical, spectroscopic, and theoretical data shows that Mn(II) complex and Ni(II) complexes (**1** and **2**) have distorted octahedral geometry around metal ion while other complexes (**3**-**5**) have distorted square pyramidal geometry. On the other hand, superoxide radical ($O_2^{\cdot -}$) scavenging activity studies revealed that all the complexes have SOD mimicking activity with IC_{50} values ranged from 2.02 to 8.36, distorted square pyramidal complexes are more active than distorted octahedral complexes and the Cu(II) complex (**4**) has found the most active. The activities of the complexes are lower than the native enzyme but higher than some reported complexes [39,40].

Acknowledgments

The numerical calculations reported in this paper were performed at TUBITAK ULAKBIM, High Performance, and Grid Computing Center (TRUBA Resources).

CRediT author statement

Kerim Serbest: Conceptualization, Methodology, Writing, Supervision, Reviewing and Editing **Turan Dural**: Investigation, **Mustafa Emirik:** Software, Theoretical calculations **Ali Zengin:** Investigation **Özlem Faiz:** Investigation of biological activity, writing

Declaration of interests

☒ The authors declare that they have no known competing financial interests or personal relationships that could have appeared to influence the work reported in this paper.

☐The authors declare the following financial interests/personal relationships which may be considered as potential competing interests:

References

[1] M. Sarigul, P. Deveci, M. Kose, U. Arslan, H. Türk Dagi, M. Kurtoglu, New tridentate azo–azomethines and their copper(II) complexes: Synthesis, solvent effect on tautomerism, electrochemical and biological studies, J. Mol. Struct. 1096 (2015) 64–73. doi:10.1016/j.molstruc.2015.04.043.

[2] M.R. Lutfor, G. Hegde, S. Kumar, C. Tschierske, V.G. Chigrinov, Synthesis and characterization of bent-shaped azobenzene monomers: Guest–host effects in liquid crystals with azo dyes for optical image storage devices, Opt. Mater. (Amst). 32 (2009) 176–183. doi:10.1016/j.optmat.2009.07.006.

[3] E. İspir, The synthesis, characterization, electrochemical character, catalytic and antimicrobial activity of novel, azo-containing Schiff bases and their metal complexes, Dye. Pigment. 82 (2009) 13–19. doi:10.1016/j.dyepig.2008.09.019.

[4] K. Bujak, A. Wasiak, A. Sobolewska, S. Bartkiewicz, J.G. Malecki, J.E. Nycz, E. Schab-Balcerzak, J. Konieczkowska, A family of azoquinoline derivatives: Effect of the substituent at azo linkage on thermal cis-trans isomerization based on an experimental and computational approach, Dye. Pigment. 175 (2020) 108151. doi:10.1016/j.dyepig.2019.108151.

[5] S. Menati, A. Azadbakht, R. Azadbakht, A. Taeb, A. Kakanejadifard, Synthesis,

characterization, and electrochemical study of some novel, azo-containing Schiff bases and their Ni(II) complexes, Dye. Pigment. 98 (2013) 499–506. doi:10.1016/j.dyepig.2013.04.009.

[6] M.S. Masoud, A.M. Beltagi, H.A. Moutawa, Synthesis, spectral, molecular modeling, thermal analysis studies of orange (II) complexes, J. Mol. Struct. 1175 (2019) 335–345. doi:10.1016/j.molstruc.2018.07.094.

[7] A. Bergamo, P.J. Dyson, G. Sava, The mechanism of tumour cell death by metal-based anticancer drugs is not only a matter of DNA interactions, Coord. Chem. Rev. 360 (2018) 17–33. doi:10.1016/j.ccr.2018.01.009.

[8] C.R. Luman, F.N. Castellano, Phenanthroline Ligands, in: Compr. Coord. Chem. II, Elsevier, 2003: pp. 25–39. doi:10.1016/B0-08-043748-6/01202-0.

[9] G. Accorsi, A. Listorti, K. Yoosaf, N. Armaroli, 1,10-Phenanthrolines: versatile building blocks for luminescent molecules, materials and metal complexes, Chem. Soc. Rev. 38 (2009) 1690. doi:10.1039/b806408n.

[10] A. Bencini, V. Lippolis, 1,10-Phenanthroline: A versatile building block for the construction of ligands for various purposes, Coord. Chem. Rev. 254 (2010) 2096–2180. doi:10.1016/j.ccr.2010.04.008.

[11] P.S. Hume, K.S. Anseth, Polymerizable superoxide dismutase mimetic protects cells encapsulated in poly(ethylene glycol) hydrogels from reactive oxygen species-mediated damage, J. Biomed. Mater. Res. Part A. 99A (2011) 29–37. doi:10.1002/jbm.a.33160.

[12] M. Puchoňová, J. Švorec, Ľ. Švorc, J. Pavlik, M. Mazúr, Ľ. Dlháň, Z. Růžičková, J. Moncoľ, D. Valigura, Synthesis, spectral, magnetic properties, electrochemical

evaluation and SOD mimetic activity of four mixed-ligand Cu(II) complexes, Inorganica Chim. Acta. 455 (2017) 298–306. doi:10.1016/j.ica.2016.10.034.

[13] H. Phetmung, T. Runpet, N. Choosiri, Roles of a unique apical salicylate ligand of neutral [Cu(phen) (Hsal)2(H2O)] to coordination mode, geometry, weak interactions, thermal analysis and spectroscopy, J. Mol. Struct. 1178 (2019) 500–507. doi:10.1016/j.molstruc.2018.10.041.

[14] D.P. Riley, Functional Mimics of Superoxide Dismutase Enzymes as Therapeutic Agents, Chem. Rev. 99 (1999) 2573–2588. doi:10.1021/cr980432g.

[15] T.A. Jackson, A. Karapetian, A.-F. Miller, T.C. Brunold, Spectroscopic and Computational Studies of the Azide-Adduct of Manganese Superoxide Dismutase: Definitive Assignment of the Ligand Responsible for the Low-Temperature Thermochromism, J. Am. Chem. Soc. 126 (2004) 12477–12491. doi:10.1021/ja0482583.

[16] K. Serbest, A. Özen, Y. Ünver, M. Er, İ. Değirmencioğlu, K. Sancak, Spectroscopic and theoretical study of 1,2,4-triazole-3-one based salicylaldimine complexes and evaluation of superoxide-scavenging properties, J. Mol. Struct. 922 (2009) 1–10. doi:http://dx.doi.org/10.1016/j.molstruc.2009.02.001.

[17] S. Güner, S. Karaböcek, I. Kaklikkaya, Models for Superoxide Dismutases: Characterization of Mononuclear Cu(II), Fe(III), and Mn(II) Complexes with 4′,5′-Bis(salicylideneimino)benzo-15-crown-5, Bioorg. Med. Chem. 7 (1999) 329–333. doi:10.1016/S0968-0896(98)00240-5.

[18] M. ÇOL AYVAZ, İ. TURAN, B. DURAL, S. DEMİR, K. KARAOĞLU, Y. ALİYAZICIOĞLU, K. SERBEST, Synthesis, in vitro DNA interactions, cytotoxicities,

antioxidative activities, and topoisomerase inhibition potentials of Mn(II), Co(II), Ni(II), Cu(II), and Zn(II) complexes with azo-oxime ligands, TURKISH J. Chem. 41 (2017) 728–747. doi:10.3906/kim-1612-53.

[19] R.N. Patel, A. Singh, K.K. Shukla, D.K. Patel, V.P. Sondhiya, S. Dwivedi, Synthesis, spectral and structural study of sulfur-containing copper(II) complexes, J. Sulfur Chem. 31 (2010) 299–313. doi:10.1080/17415993.2010.499567.

[20] E.M. Niecy, L.P. Nitha, R. Aswathy, B. Sindhukumari, K. Mohanan, Synthesis, characterization, antibacterial, DNA cleavage and SOD activities of some 3d metal complexes of ethyl[2-(1H-indol-3-yl)methyleneamino]-4,5,6,7-tetrahydrobenzo[b]thiophene-3-carboxylate, Med. Chem. Res. 24 (2015) 63–77. doi:10.1007/s00044-014-1099-5.

[21] Y. Singh, R.N. Patel, Y.P. Singh, A.K. Patel, N. Patel, R. Singh, R.J. Butcher, J.P. Jasinski, E. Colacio, M.A. Palacios, Unprecedented tetranuclear complexes with "weighing balance shaped" topology: single crystal structures, unusual EPR spectra, magnetic properties and antioxidant activity, Dalt. Trans. 46 (2017) 11860–11874. doi:10.1039/C7DT02595E.

[22] M.J. Frisch, G.W. Trucks, H.B. Schlegel, G.E. Scuseria, M.A. Robb, J.R. Cheeseman, V.B.G. Scalmani, B. Mennucci, G.A. Petersson, H. Nakatsuji, M. Caricato, X. Li, H.P. Hratchian, A.F. Izmaylov, J. Bloino, G. Zheng, J.L. Sonnenberg, M. Hada, M. Ehara, K. Toyota, R. Fukuda, J. Hasegawa, M. Ishida, T. Nakajima, O.K.Y. Honda, H. Nakai, T. Vreven, J.A. Montgomery Jr, J.E. Peralta, F. Ogliaro, M. Bearpark, J.J. Heyd, E. Brothers, K.N. Kudin, V.N. Staroverov, R. Kobayashi, J. Normand, K. Raghavachari, A. Rendell, J.C. Burant, S.S. Iyengar, J. Tomasi, M. Cossi, N. Rega, J.M. Millam, M. Klene, J.E. Knox, J.B. Cross, V. Bakken, C. Adamo, J. Jaramillo, R. Gomperts, R.E.

Stratmann, O. Yazyev, A.J. Austin, R. Cammi, C. Pomelli, J.W. Ochterski, R.L. Martin, K. Morokuma, V.G. Zakrzewski, G.A. Voth, P. Salvador, J.J. Dannenberg, S. Dapprich, A.D. Daniels, O. Farkas, J.B. Foresman, J.V. Ortiz, J. Cioslowski, D.J. Fox, Gaussian 09, revision A.02 Gaussian, Inc, Wallingford, 2009.

[23] P.J. Hay, W.R. Wadt, Ab initio effective core potentials for molecular calculations. Potentials for the transition metal atoms Sc to Hg, J. Chem. Phys. 82 (1985).

[24] M. H. Jamroz, Vibrational Energy Distribution Analysis: VEDA 4 Program, Warsaw, (2004).

[25] J. Tomasi, B. Mennucci, R. Cammi, Quantum Mechanical Continuum Solvation Models, Chem. Rev. 105 (2005) 2999–3094. doi:10.1021/cr9904009.

[26] N.M. O'boyle, A.L. Tenderholt, K.M. Langner, cclib: A library for package-independent computational chemistry algorithms, J. Comput. Chem. 29 (2008) 839–845. doi:10.1002/jcc.20823.

[27] K. Serbest, K. Karaoğlu, M. Erman, M. Er, I. Değirmencioğlu, Synthesis, characterization and properties of tetra((1-hydroxyimino-methylnaphthalen-2-yloxy)methyl)ethene and its homo-dinuclear metal complexes: a combined experimental and theoretical investigation., Spectrochim. Acta. A. Mol. Biomol. Spectrosc. 77 (2010) 643–51. doi:10.1016/j.saa.2010.07.002.

[28] M. Emirik, K. Karaoğlu, K. Serbest, U. Çoruh, E.M. Vazquez Lopez, Two novel unsymmetrical ferrocene based azines and their complexing abilities towards Cu(II): Spectroscopy, crystal structure, electrochemistry and DFT calculations, Polyhedron. 88 (2015) 182–189. doi:10.1016/j.poly.2014.12.044.

[29] T. Madanhire, M.C. Pereira, H. Davids, E.C. Hosten, A. Abrahams, Lanthanide(III)

complexes with N-(2,6-dimethylphenyl)oxamate and 1,10-phenanthroline: Synthesis, characterisation and cytotoxicity against MCF-7, HEC-1A and THP-1 cell lines, Polyhedron. 189 (2020) 114713. doi:10.1016/j.poly.2020.114713.

[30] S.Ž. Đurić, M. Mojicevic, S. Vojnovic, H. Wadepohl, T.P. Andrejević, N.L. Stevanović, J. Nikodinovic-Runic, M.I. Djuran, B.Đ. Glišić, Silver(I) complexes with 1,10-phenanthroline-based ligands: The influence of epoxide function on the complex structure and biological activity, Inorganica Chim. Acta. 502 (2020) 119357. doi:10.1016/j.ica.2019.119357.

[31] N.M.N. Gowda, S.B. Naikar, G.K.N. Reddy, Perchlorate Ion Complexes, in: 1984: pp. 255–299. doi:10.1016/S0898-8838(08)60210-X.

[32] B.J. Hathaway, A.E. Underhill, 592. The infrared spectra of some transition-metal perchlorates, J. Chem. Soc. (1961) 3091. doi:10.1039/jr9610003091.

[33] M. Ghosh, P. Biswas, U. Flörke, Structural, spectroscopic and redox properties of transition metal complexes of dipyrido[3,2-f:2′,3′-h]-quinoxaline (dpq), Polyhedron. 26 (2007) 3750–3762. doi:10.1016/j.poly.2007.04.014.

[34] R.K. Gopal, S. Elumalai, Industrial Production of Superoxide Dismutase (SOD): A Mini Review, J. Probiotics Heal. 05 (2017). doi:10.4172/2329-8901.1000179.

[35] N. V. Loginova, H.I. Harbatsevich, T. V. Koval`chuk, N.P. Osipovich, Y.S. Halauko, Y. V. Faletrov, G.A. Ksendzova, S.I. Stakhevich, I.I. Azarko, Antimicrobial and SOD-Like Activities of Novel Zinc(II) Complexes with Redox-Active Sterically Hindered Diphenols, Curr. Bioact. Compd. 14 (2018) 397–411. doi:10.2174/1573407213666170614110911.

[36] Z.A. Siddiqi, M. Shahid, M. Khalid, S. Kumar, Antimicrobial and SOD activities of

novel transition metal ternary complexes of iminodiacetic acid containing α-diimine as auxiliary ligand, Eur. J. Med. Chem. 44 (2009) 2517–2522. doi:10.1016/j.ejmech.2009.01.025.

[37] S. Bharti, M. Choudhary, B. Mohan, S.P. Rawat, S.R. Sharma, K. Ahmad, Syntheses, spectroscopic characterization, SOD-like properties and antibacterial activities of dimer copper (II) and nickel (II) complexes based on imine ligands containing 2-aminothiophenol moiety: X-ray crystal structure determination of disulfide Schif, J. Mol. Struct. 1164 (2018) 137–154. doi:10.1016/j.molstruc.2018.03.041.

[38] L.-Q. Chai, H.-S. Zhang, J.-J. Huang, Y.-L. Zhang, An unexpected Schiff base-type Ni(II) complex: Synthesis, crystal structures, fluorescence, electrochemical property and SOD-like activities, Spectrochim. Acta Part A Mol. Biomol. Spectrosc. 137 (2015) 661–669. doi:10.1016/j.saa.2014.08.084.

[39] E. Santi, I. Viera, A. Mombrú, J. Castiglioni, E.J. Baran, M.H. Torre, Synthesis and Characterization of Heteroleptic Copper and Zinc Complexes with Saccharinate and Aminoacids. Evaluation of SOD-like Activity of the Copper Complexes, Biol. Trace Elem. Res. 143 (2011) 1843–1855. doi:10.1007/s12011-011-8992-2.

[40] R.N. Patel, N. Singh, V.L.N. Gundla, Synthesis, characterization and superoxide dismutase activity of some octahedral nickel(II) complexes, Polyhedron. 26 (2007) 757–762. doi:10.1016/j.poly.2006.09.041.

K. Serbest

T. Dural

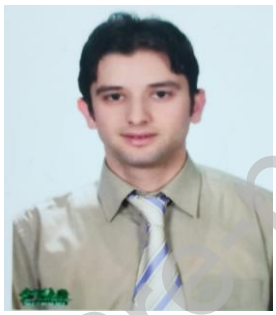

A. Zengin

M. Emirik

Ö. Faiz